Published on Acta Materialia, **55** [7] (2007) 2229-2238 ©by Elsevier Ltd. DOI 10.1016/j.actamat.2006.11.008

Crystal structural and optical properties of Cr-doped $Y_2Ti_2O_7$ and $Y_2Sn_2O_7$ pyrochlores

F. Matteucci [a], G. Cruciani [b], M. Dondi [a], G. Baldi [c], A. Barzanti [c]

[a] *ISTEC-CNR, Institute of Science and Technology for Ceramics, Via Granarolo 64, 48018 Faenza, Italy*

[b] *Department of Earth Sciences, University of Ferrara, Via Saragat 1, 44100 Ferrara, Italy*

[c] *CE.RI.COL., Colorobbia Italia spa, Via Pietramarina 123, 50053 Vinci, Italy*

Abstract

Pyrochlore-type [$A^{VIII}{}_2B^{VI}{}_2O_6O$] rare earth stannates (PS) and titanates (PT), doped with increasing amount of Cr, develop colours ranging from magenta to brown. Combined X-ray and neutron diffraction data revealed that Cr solubility in both pyrochlores is very limited, i.e. 0.07 atoms/formula unit in PS and 0.06 atoms/formula unit in PT. A further increase in the Cr amount determines the formation of the $YCrO_3$ perovskite. Diffuse reflectance spectroscopy data showed that the optical properties of Cr-doped yttrium titanates and stannates are rather similar, being the final powders colour due to the overlapping peaks of Cr^{4+} in the octahedral site of the pyrochlore and of Cr^{3+} in the ternary perovskite. The oxygen occupancy refinement showed that no anion vacancies are formed upon Cr substitution for Sn^{4+} or Ti^{4+}, implying that such a charge compensation mechanism does not occur, confirming that chromium in titanate and stannate pyrochlores is mainly in a tetravalent state.

Keywords: Optical properties, Neutron diffraction, Optical spectroscopy, Pyrochlore, X-ray diffraction

1. Introduction

Compounds exhibiting the pyrochlore structure have been extensively investigated, especially for their properties of anion and mixed conduction [1,2], magneto-resistance [3] and superconductivity [4] due to their ability to incorporate an incredibly wide range of elements. A great deal of applications have been envisaged, including sensors and transistors [5], dielectrics and fast ion conductors [1,6], electrocatalysts [7] or actinide host phase for nuclear waste encapsulation [8]. In particular, titanate and stannate pyrochlores have been synthesised since forty years [9-11], so that a deep knowledge of their structural trends [12], thermodynamic properties [13], disorder [14,15] and non-stoichiometry [16] has been developed.

The cubic pyrochlore structure (space group Fd-3m, Z=8), with general formula $A^{3+}{}_2B^{4+}{}_2O_6O'$, can be described as a defective fluorite solid solution, where cations form a face-centred cubic array and 1/8 of anions are removed to ensure the charge neutrality. These oxygen vacancies are ordered as well as A and B cations are alternated in <110> rows, so producing a doubling of fluorite lattice parameters (Fd-3m, Z=4) [17]. In this way, five unique crystallographic positions are available in the Wyckoff notation: 16d for A cations, 16c for B cations, 48f for O, 8b for O', while 8a sites (1/8, 1/8, 1/8) are vacant [14]. Oxygen ions in the 8b sites are in an undisturbed position (3/8, 3/8, 3/8) with respect to the fluorite structure and are tetrahedrically coordinated by A cations. In contrast, oxygen ions at 48f (x, 1/8, 1/8) are displaced toward the neighbouring vacant 8a sites and bonded to two A and two B cations. The A cations occupy an axially compressed scalenohedron coordinated by six O (8b) and two O' (48f) atoms, these latter being at a slightly shorter

distance from the central cation. The 6-fold coordinated B cations are at equivalent distances from the O (48f) oxygen atoms in trigonal antiprisms, with a point symmetry -3m (D_{3d}). Hence, the A-O and B-O distances depend on both lattice parameter and oxygen positional parameter [1,12,16]. As an alternative description, the $A^{3+}{}_2B^{4+}{}_2O_6O'$ pyrochlore structure can be also viewed as made up of two interpenetrating covalent networks, $(A_2O')^{4+}$ and $(BO_3)^{4-}$, that are linked by the O^{2-} anions of the $(BO_3)^{4-}$ network mainly via ionic bonding [18].

The titanate and stannate pyrochlores are promising candidates for ceramic pigments, fulfilling the basic requirements of rather high melting point (i.e. ~1600 °C), high refractive index ($2.0<n<2.2$) and ability to host first-row transition metal ions in their crystal lattice, especially in the octahedrally coordinated site. Although an interesting yellow-colored pigment was already developed by doping yttrium stannate with vanadium and calcium [19], current research is focussed on discovering red-colored compounds suitable for high temperature ceramic applications [20-22]. From this standpoint, attempts have been recently made to get red shades by doping with chromium both yttrium stannate and neodynium zirconate [23-25]. These investigations revealed that the chromophore ion in stannate pyrochlores is Cr^{4+} [25] showing strong analogies with other Cr-doped tin compounds, such as cassiterite and malayaite [26,27].

However, the coloring mechanism of these pyrochlores is still not fully understood – particularly chromatic trends for growing amounts of chromium – and the possible role of non-stoichiometry or oxygen vacancies, which cannot ruled out altogether, has not been duly investigated up to now. Besides, a thoroughful characterisation of optical properties is still lacking. Therefore, the main goal of the present paper is to appraise the relationships between crystal structure and optical properties of both yttrium titanate and yttrium stannate pyrochlores over a wide range of Cr additions, with special emphasis on coloration mechanisms. For this purpose, neutron diffraction, X-ray diffraction and diffuse reflectance spectroscopy were combined in order to get insights on the effect of stoichiometry and chromium solubility on color of pyrochlore-based ceramic pigments.

2. Experimental

2.1. Powders preparation

Along with the undoped samples, the Cr-doped titanates and stannates pyrochlore series, hereafter named PT and PS respectively, were designed according with the following formulations: $Y_2A_{2-x}B_xO_6O'$, where A = Ti, Sn; B = Cr; x = 0, 0.02, 0.07, 0.25, 0.50, 0,75, 1. Reagent-grade oxides with particle size distribution of 20-30 μ m – ytrria (Y_2O_3), anatase (TiO_2), cassiterite (SnO_2) and eskolaite (Cr_2O_3) - were used as raw materials. No mineraliser was added. These samples are hereafter named with the series label followed by the Cr-doping amount multiplied by 100.

The samples were prepared by conventional mixed metal-oxide methods in alumina crucible in an electric furnace with a heating rate of 225°C/h up to 1350°C a soaking time of 24 hours and natural cooling.

2.2. Characterization techniques

X-ray powder diffraction was performed on all the samples by a Philips PW1820/00 goniometer using graphite-monochromated Cu $K_{\alpha\,1,2}$ radiation, 15-130 °2θ measuring range, scan rate 0.02 °2θ , 10 s per step. The neutron powder diffraction experiments, performed only on the Cr-doped samples, were undertaken with the high-flux, high resolution diffractometer D2B (λ =1.59432 Å), at the Institute Laue Langevin, Grenoble, France. Approximately 10 g of each sample were loaded in a cylindrical vanadium samples can and the data were collected for the angular range 2θ = 0–159.95° in steps of

0.05°. Full diffraction profiles were obtained with counting times of ≅ 6 hours at room temperature. The structural refinements were performed combining X-ray and neutron data by the Rietveld method with the GSAS-EXPGUI software package [28,29]. Starting atomic parameters in the *Fd-3m* space group for the PS and PT series were taken from Ismunandar et al. [7] and Chtoun et al. [30] respectively, and used for all refinements. As far as the $YCrO_3$ is concerned, its starting atomic parameters in the *Pnma* space group were taken from Cruciani et al. [31]. Up to 45 independent variables were refined, including: scale-factors, zero-point, 10 coefficients of the shifted Chebyschev function to fit the background, pyrochlore and perovskite cell dimensions, atomic positions, isotropic displacement parameters, and profile coefficients: 3 gaussian (G_U, G_V and G_W) and 2 lorentzian terms (L_X, L_Y). The number of variables and observations as well as the figures-of-merit of all refinements are summarised in Tables 1 and 2 and.
UV-visible-NIR spectroscopy was performed by diffuse reflectance with integrating sphere (Perkin Elmer λ 35) in the 300-1100 nm range, step 0.3 nm, using $BaSO_4$ as a reference. The positions of the main absorbance peaks in the optical spectra were determined through a deconvolution procedure (PFM, OriginLab), that allowed to obtain averaged values of crystal field strength (Dq_{cub}), peak splitting (δ), crystal field stabilization energy (CFSE), Racah B parameter (both B_{35} and B_{55} for perovskite) and nephelauxetic ratio β (i.e. B/B_0, where B is experimental and B_0 is the value of the free ion [32]). Dq was estimated by the Tanabe-Sugano diagrams and fitting spin-allowed transitions; B_{35} and B_{55} were calculated by spin-allowed and spin-forbidden transitions, respectively [32-33]; δ was measured as FWHM on some peaks of optical spectra; the crystal field stabilization energy (CFSE) was calculated by Dq values [34].

3. Results and discussion

3.1. Crystal structure modifications

The phase composition, unit cell parameters and atomic coordinates of the PT and PS samples are listed in Table 1 and 2, respectively.
The structural changes related to the increasing level of Cr in the PS series are better understood by analogy with those occurring when increasingly smaller Rare Earth cations are replaced for Y in stannate pyrochlores (hereafter referred to as 'REE-stannates') [12]. In both cases a net decrease of the pyrochlore unit cell volume is expected based on the decreasing average ionic radii in the B or A sites. Figure 1 shows that the unit cell decreases while the refined Cr occupancy increases, as expected on the basis of the ionic radii (*r.i.* of six-coordinated Cr^{4+} 56 pm, Cr^{3+} 62 pm and Sn^{4+} 69 pm [35]); this trend is not linear, in agreement with previous findings on Cr substituted Y-stannates [24]. In order to explain such a non-linear trend, the relationship between the average refined <B-O> distance and the cell parameter must be considered (Fig. 2). As expected, the <B-O> distance decreases with increasing Cr content (i.e. decreasing cell parameter). However, it appears that the bond distance contraction reaches a limit at about 204 pm. This is very close to the limit also found in REE-stannates on decreasing cell parameter caused by decreasing REE ionic radii (see Figures 3 and 4 in [12]).
The occurrence of a lower limit (about 204 pm) on the <B-O> distance in Y-stannates upon substitutions in the A or B sub-networks can be interpreted considering that in the PS0 sample (pure Sn-term) all the Sn-O distances are already much shorter than the sum of the ionic radii of $^{[4]}O^{2-}$ (138 pm) and $^{[6]}Sn^{4+}$ (69 pm) [35]. This means that the SnO_6 octahedron experiences a quite strong compression, which is further increased by incorporation of Cr into it.

In fact the shorter O-O distance decreases from 265.9 pm to 265.1 pm as Cr content increases. The latter value is very close to 265.0 pm which is the length of the O-O edge in

a silicon tetrahedron. On this basis and taking into account that as the <Sn-O> distance approaches the 204 pm limit the unit cell parameter also reaches its minimum value (in PS series, about 103.6 pm), we can speculate that the non-linear trend of the cell parameter might be due to the exponential law relating potential energy and interatomic distance of the O-O edge [36].

A further peculiar behaviour of the pyrochlore structure is the direct correlation between <A-O> and <B-O> distances, as also observed in our PS series (see Figure 3); in fact, a shrinking of one sub-network (*e.g.* the A_2O' network) causes the contraction of the other and vice versa always leading to an overall shrinkage. As far as this feature is concerned, the perovskite structure behaves in a different way; in fact, the effects of A and B distance variations tend to be compensated each other [31]. In order to assess how the interconnection between the two pyrochlore sub-networks accommodates the overall shrinkage promoted inside one or the other, the variation of the *x* coordinate of the O oxygen (*i.e.* the only variable positional parameter in pyrochlore structure) can be evaluated. In fact the two distinct sub-network are connected via the O oxygen (bonded twice both to A and B cations). Figure 4 shows that in the PS series the variation range of this parameter is very small, being in the 0.3366-0.3364 interval. An overall direct relationship of the *x* vs. the unit cell parameter can be observed, although its variation is not quite linear as found by [12]. It is noteworthy that, contrary to PS series, in REE stannates the relationship *x*(O) vs. *a*-axis shows an inverse trend (see Figure 4 in [12]). This difference is not surprising because the shrinking affecting one or the other sub-network implies that the O^{2-} anion linking them can be displaced either in one direction or the other. In particular, as the unit cell volume decreases, for the PS series it is increasingly shifted towards the vacant 8a (1/8, 1/8, 1/8) site whereas in the case of REE stannate series [12] it moves away from the same site. The *x*(O) coordinate can also be used to gain insights on the pyrocholre lattice stability. In fact, the lower the *x*(O) value the more the six coordinated site approaches a regular octahedron, thus stabilizing the pyrochlore structure [1]. On this basis, it could be inferred that the addition of Cr to the batch synthesis has the effect to enhance the pyrochlore stability. This would also agree with the argument that a change of the radius ratio $R = r^{3+}/r^{4+}$ from 1.48 to 1.50 as the Cr content increases in the PS series (the range for stable pyrochlore<s is 1.46-1.80) would increase the pyrochlore lattice stability [1]. However, as discussed in a following section, the pyrochlore stability appears to scale inversely with Cr content suggesting that thermodynamic issues likely override geometrical constraints. The opposite trends of the *x*(O) vs. *a*-axis variation in Cr- and REE-substituted Y-stannates are also reflected in the opposite behaviour of both the relationships of O-B-O and B-O-B bond angles vs. the unit cell parameter. This is confirmed by comparing Figure 5a,b to Figure 6 of Kennedy et al. [12]. Considering the variation of bond valence sums (BVSs) in REE stannates, the above authors described an increase of the electron density at the Sn nuclei (thus an associated decreasing level of covalency in the Sn-O bonding) as the *a* parameter decreased due to radii contraction along the lanthanide series in $LnSn_2O_7$. The change of BVSs at different sites in the PS series is shown in Figure 6. Despite the range of variation is clearly much narrower (therefore less significant) than in [12], it can be noted that the trends of A and B site BVSs, still mirrored each other, are reversed with respect to REE-stannates. The BVS of A site increases while that of B site decreases as a function of the shortening *a*-axis (Cr increase). Furthermore, unlike in REE-stannates, the associated remarkable variation of the O' BVS is not found in PS series.

As far as the PT series is concerned, the trends described above become less clearly defined (see Table 1). In fact the variations of the unit cell parameter versus the Cr doping amount and the mean B-O distance are not as linear as the one of the PS series: in particular, an anomalous value for the sample PT25 was found and confirmed even after repeating twice the sample preparation. We do not have a definite explanation to justify the

less regular behaviour of the PT series compared to the PS series. Very likely, it could be simply due to the smaller difference of ionic radii between Cr^{4+} and Ti^{4+} compared to Cr^{4+} and Sn^{4+}. It implies that the structural correlations would be masked to a larger extent by the standard errors on results. Anyway, some trends observed in the PS series, such as the direct correlation between <A-O> and <B-O> and the inverse correlation between the x(O) and the unit cell parameter, still seem to be confirmed in the PT series suggesting that the same model of structural modifications upon Cr incorporation might also hold in the pyrochlore Y-titanates. Unfortunately no structural data are available in the literature on REE-substituted titanates to allow comparison.
The refined occupancies of O and O' oxygen sites in both series deserve a specific comment since the appraisal of the possible occurrence of anion vacancies was one of our initial goals. From Tables 1 and 2 it is clear that no evidence for oxygen deficiencies is found, though it was expected to take place in particular at the O (48f) sites in the case of Cr^{3+} for Sn^{4+} or Ti^{4+} substitution, as a function of the increasing amount of Cr incorporated in both Y-stannates and Y-titanates. These findings provide further support for the tetravalent state of chromium in pyrochlore pigments, in agreement with optical spectroscopy data, as described later, and literature results [24].

3.2. Phase composition and pyrochlore stability

As far as the phase composition is concerned, the Cr solubility is 0.07 a.p.f.u. in the PS series and approximately 0.06 a.p.f.u. in the PT series. These values are much smaller than what found in the literature [23-25] for the stannates and justify the noticeably high amount of perovskite YCrO3 as secondary phase whenever higher amounts of Cr are used in the batch (Fig. 7). In reality, this discrepancy is only apparent, as the first perovskite formation in the PS series is detected for x=0.25 in the present study and x=0.20 by Navarrete *et al.* [25]. Pavlov *et al.* [23-24] found perovskite only starting from x=0.50, probably because of their higher detection limit with respect to our XRD-ND combined approach. In fact, the pyrochlore structure cannot host a high Cr amount, as the necessity to recur to both high pressure and high temperature to synthesize $Y_2Cr_2O_7$ confirms [37], due to the too small ionic radius of Cr^{4+} that induces a R (r^{3+}/r^{4+}) value of 1.85 (out of the pyrochlore stability) [1]. This seems to be confirmed by the increase of the line broadening measured by its FWHM (full width half maximum) which can be related to the decrease of the crystallite size or to the increase of the lattice strain in both the PS and PT series as the Cr content increases.
The reason of the higher Cr solubility in the PS series, nevertheless the ionic radii difference between Sn-Ti and Cr would let suppose a higher solubility in the PT series, is to be found in energetic considerations. In fact, the PT series is more stable than the PS one having a higher negative reaction enthalpy; therefore, more energy is required to introduce a defect, *i.e.* Cr doping, in the PT series [14, 38].
These findings suggest that thermodynamical issues might override the geometrical stability rules of pyrochlores.

3.3. Optical properties

The optical properties of Cr-doped yttrium titanates and stannates are rather similar, as shown by diffuse reflectance spectra (Figs. 8A, 8B). The main feature is a sharp band at 16000-18000 cm^{-1} gently dipping to a minimum of absorbance at ~13000 cm^{-1}. As transmitted light is to a large extent in the 14000-16000 cm^{-1} range (i.e. approximately 600-700 nm) these pigments exhibit red shades. Increasing the amount of chromium, several changes occurred in both series (Figs. 8A, 8B):

- strong absorbance growth,
- steeper slope of the main band,

– minor ripples at ~11000 cm^{-1} and ~25000 cm^{-1} become more intense,
– a second minimum of absorbance at ~22000 cm^{-1} is being unresolved,
– two weak peaks appear in the 13000-15000 cm^{-1} range.

These changes are explained by different spectral contributions from the two crystalline phases present in these samples. The perovskite-free pyrochlores exhibit a spectrum with two broad bands at ~18000 cm^{-1} (ν_1) and ~26000 cm^{-1} (ν_2) plus a minor one (ν_3) at ~10500 cm^{-1} (Fig. 9a). The monophasic $YCrO_3$ spectrum is characterised by two intense bands at ~16400 cm^{-1} (ν_1) and ~22400 cm^{-1} (ν_2) associated to a couple of ripples at ~13700 cm^{-1} and ~14500 cm^{-1} (Fig. 9b) plus a lorentzian band at high energy for metal-oxygen charge transfer (MOCT). Taking these end-term features as templates, even the complex two-phases spectra were satisfactorily deconvolved in 7 gaussian bands plus a lorentzian one for MOCT (Fig. 9c). Despite the general uncertainty in deconvolving largely overlapping bands, this procedure gave a reliable response in terms of intensity ratios of the main bands of both pyrochlore and perovskite (Table 3): as a matter of fact, being ν_1/ν_2=0.34 in $YCrO_3$, values found in binary mixtures range from 0.28 to 0.37, with just one outlier (PT50). On the other hand, perovskite-free pyrochlores exhibit variable values ($0.34<\nu_1/\nu_2<0.57$); most data of binary mixes fall in this range, though some exception in the stannate series (Table 3). However, the ν_3/ν_1 ratio presents a certain increasing trend with chromium addition, easily appreciable as the fastly growing hump in the near infra-red (Figs. 8A, 8B).

The three bands of pyrochlore spectra can be attributed to d-d electronic transitions of Cr^{4+} in octahedral coordination [32, 39-40]: ν_1 and ν_2 to the spin-allowed $^3T_{1g}(^3F)\rightarrow{}^3T_{2g}(^3F)$ and $^3T_{2g}(^3P)$, respectively, while ν_3 could be due to coalesced spin-forbidden $^3T_{1g}(^3F)\rightarrow{}^1E_g+{}^1T_{2g}(^1D)$. The energy of the ν_1 and ν_2 peaks is in good agreement with the Tanabe-Sugano diagram for d^2 ions, once the electronic repulsion Racah B parameter is taken into account to adjust the energy level plot (Fig. 10). In contrast, the energy of the ν_3 band seems to be too high for such spin-forbidden transitions [32].

The occurrence of Cr^{4+} in tetrahedral coordination though widely documented in oxides and silicates [41-42] and claimed for pyrochlores [27], is improbable for both structural and spectroscopic reasons. The former because it implies localization of chromium ions in interstitial sites of a compact, face-centred array of cations as that of pyrochlore lattice; the latter because d-d transitions of tetrahedrally coordinated Cr^{4+} ions are mostly in the 12000-18000 cm^{-1} range [41-46] where our samples have their minimum absorbance.

Crystal field splitting Δ o of the octahedrally coordinated Cr4+ varies widely in titanates, from 18270 to 19730 cm-1, being roughly increasing with the amount of chromium in pyrochlore lattice, but it is quite steady in stannates, ranging from 19710 to 19840 cm-1 (Table 4). These values confirm those obtained by Pavlov *et al.* [24] and are coherent with a large set of Δ t obtained for Cr4+ in several tetrahedral sites [40-45] once the conversion Δ o=9/4 Δ t is made. However, these data are not consistent with the crystal field theory, as a larger Δ o is expected in titanate pyrochlores that have a shorter metal-oxygen bonding (B-O ~195 pm) with respect to stannates (B-O ~203 pm).

The Racah B parameter is on average 720 cm-1 in the PT series and 665 cm-1 in the PS one, exhibiting in both series a clearly increasing trend with chromium amount (Table 4). In particular, the Racah B range found in stannates (640-680 cm-1) is considerably narrower than that determined by Pavlov *et al.* [24] on the same series (589-819 cm-1); these latter data, however, were measured without taking into account the perovskite contribution to the optical spectra. The nephelauxetic ratio indicates a slightly more covalent Cr-O bonding in stannates (β =0.64) than in titanates (β =0.69). These values are higher than those determined for Cr4+ in silicate and germanate tetrahedra, *i.e.* Racah B in the 400-560 cm-1 range [42-46].

Yttrium chromium perovskite exhibits typical spectral features of octahedrally coordinated Cr^{3+}, having a d^3 electronic configuration: ¿ 1 and ▪ 2 are due to $^4A_{2g}(^4F) \rightarrow ^4T_{2g}(^4F)$ and $^4T_{1g}(^4F)$ parity-forbidden transitions, while the two weak bands at the red-IR border are related to $^4A_{2g}(^4F) \rightarrow ^2E_g(^2G)$ and $^2T_{1g}(^2G)$ spin-forbidden transitions [32-34]. The resulting spectral parameters are Δ_o=16740 cm^{-1}, Racah B_{35}=587 cm^{-1} and B_{55}=420 cm^{-1} (Table 4) confirming previous studies [39]. Corresponding nephelauxetic ratios indicate a remarkable covalency of Cr-O bonding (β 35=0.64) as well as a high polarizability of ligands (β 55=0.46) [32-33].
Optical properties of perovskite in equilibrium with pyrochlore show values of both crystal field strength and Racah B parameters that are systematically slightly lower than in YCrO3 (Table 4) thus suggesting the chance of a slightly larger octahedral site with a somehow more extended electronic cloud, that are characteristics consistent with some substitution of Ti or Sn after Cr.

4. Conclusions

Pyrochlore type rare earth stannates (PS) and titanates (PT) showed a low solubility with Cr. In the former series the reason is mainly geometrical, due to the smaller ionic radius of Cr compared to Sn that causes a too high octahedron compression. In the PT series, thermodynamical reasons can be claimed, being these pyrochlores more stable than the PS ones. Further Cr addition determined the crystallization of $YCrO_3$ as secondary phase. Optical spectroscopy data displayed the presence of two different chromium species distributed in the two crystalline phases present: Cr^{3+} in the perovskite and Cr^{4+} in the pyrochlore structure. Unit cell parameter and bond length variation, together with the full occupancy of both oxygen sites, reinforced spectroscopic results so claiming a Cr^{4+} substitution in the octahedral sites of both PT and PS series. The different colours bestowed on the PS and PT samples for increasing amount of Cr are due to the sum of the magenta colour of Cr^{4+} in the pyrochlore structure and the green colour of the Cr^{3+} in the perovskite structure.

Acknowledgement

We thank the Institute Laue-Longevin (ILL) for providing access to neutron source under the public beamtime programme (exp. No. 5-21-891). Special thanks go to D2B (high-resolution powder diffractometer) staff for the kind assistance during data collections.

References

1] M.A. Subramanian, G. Aravamudan, G.V. Subba Rao, Prog. Solid St. Chem 1983;15:55
2] O. Porat, C. Heremans, H.L Tuller, Solid State Ionics 1997;94:75
3] Y. Shimakawan, Y. Kubo, T. Manako, Nature 1996;379:53
4] M. Hanawa, Y. Muraoka, T. Tayama, T. Sakakibara, J. Yamanra, Z. Horoi, Phys. Rev. Lett. 2001;87:187
5] J.B. Goodenough, R.N. Castellano, J. Solid State Chem. 1982;44:108
6] P.P. Rao, S.J. Liji, K.R. Nair, P. Koshy, Mater. Lett. 2004;58:1924
7] Ismunandar, B.J. Kennedy, B.A. Hunter, T., J. Solid State Chem. 1997;131:317
8] E.J. Harvey, K.R. Whittle, G.R. Lumpkin, R.I. Smith, S.A.T. Redfern, J. Solid State Chem. 2005;178:800
9] L.H. Brixner, Mater. Res. Bull. 1984;19:143
10] F. Brisse, O. Knop, Can. J. Chem. 1968;46:859
11] O. Knop, F. Brisse, Can. J. Chem. 1969;47:971
12] B.J. Kennedy, B.A. Hunter, C.J. Howard, J. Solid State Chem. 1997;130:58
13] K.B. Helean, S.V. Ushakov, C.E. Brown, A. Navrotsky, J. Lian, R.C. Ewing, J.M. Farmer, L.A. Boatner, J. Solid State Chem. 2004;177:1858
14] L. Minervini, R.W. Grimes, J. Am. Ceram. Soc. 2000;83:1873
15] C. Heremans, B.J. Wuensch, J.K. Staick, E. Prince, J. Solid State Chem. 1995;117:108
16] C.R. Stanek, L. Minervini, R.W. Grimes, J. Am. Ceram. Soc. 2002;85.2792.
17] E. Aleshin, R. Roy, J. Am. Ceram. Soc. 1962;45:18
18] M.A. Subramanian, AW. Slieght, Handbook Phys. Chem. Rare Earths, 1993;16:225
19] S. Ishida, F. Ren, N. Takeuchi, J. Am. Ceram. Soc. 1993;76:2644
20] F. Bondioli, T. Manfredini, C. Siligardi, A.M. Ferrari, J. Eur. Ceram. Soc. 2004;24:3593
21] F. Bondioli, T. Manfredini, Am. Ceram. Soc. Bull. 2000;2:68
22] F. Matteucci, C. Lepri Neto, M. Dondi, G. Cruciani, G. Baldi, A.O. Boschi, Adv. Appl. Ceram. 2006;105:99
23] R.S. Pavlov, V. Blasco, J.M. Hoemberger, J.B. Carda, Key Eng. Mater. 2002;206-213:2137
24] R.S. Pavlov, J.B. Carda, V.B. Marza, J. Am. Ceram. Soc. 2002;85:1197
25] E. LÛpez Navarrete, V.M. Orera, F.J. Lazaro, J.B. Carda, M. Ocana, J. Am. Ceram. Soc. 2004;87:2108.
26] A.M. Heyns, P.M. Harden, J. Phys. Chem. Solids 1999;60:277.
27] E. LÛpez Navarrete, A. Caballero, V.M. Orera, F.J. Lazaro, M. Ocana, Acta Mater. 2003;51:2371
28] Larson, A.C., Von Dreele, R.B., Los Alamos National Laboratory Report LAUR 2000;86
29] Toby, B.H., J. Appl. Crystallogr. 2001;34:210
30] E. Chtoun, L. Hanebali, P. Garnier, J.M. Kiat, Eur. J. Solid State Inorg. Chem. 1997;34:553
31] G. Cruciani, F. Matteucci, M. Dondi, G. Baldi, A. Barzanti, Z. Krist. 2005;200:930
32] A.B.P. Lever, Inorganic electronic spectroscopy, Amsterdam, Elsevier, 2nd edition, 1984.
33] M. Wildner, M. Andrut, C.Z. Rudowicz, in: A. Beran, E. Libowitzky, editors. Optical absorption spectroscopy in geosciences, Part I: Basic concepts of crystal field theory, EMU Notes in Mineralogy, Vol.6. Eotvos University Press, 2004, p.93.
34] R.G. Burns, Mineralogical applications of crystal field theory, Cambridge University Press, 2nd edition, 1993.
35] R.D. Shannon, Acta Crystallogr. 1976;A32:751
36] M. O'Keeffe, A Navrotsky, A.N. Bloch, Structure and Bonding in crystals, Academic Press, 1981.
37] J. Pannetier, J. Phys. Chem. Solids 1973;34:583
38] P.J. Wilde, C.R.A. Catlow, Solid State Ionics 1998;112:173
39] R.S. Pavlov, V.B. Marza, J.B. Carda, J. Mat. Chem. 2002;12:2825
40] G.C. Allen, K.D. Warren, Structure and Bonding 1971;9:49
41] R. Feldman, Y. Shimony, Z. Burshtein, Opt. Mater. 2003;24:333
42] D. Reinen, U. Kesper, M. Atanasov, J. Roos, Inorg. Chem. 1995;34:184
43] A. Belletti, R. Barromei, L. Oleari, Inorg. Chim. Acta 1995;235:349
44] C. Deka, M. Bass, B.H.T. Chai, Y. Shimony, J. Opt. Soc. Am. B 1993;10:1499
45] M.Y. Sharonov, A.B. Bykov, V. Petricevic, R.R. Alfano, Opt. Comm. 2004;231:273
46] M.F. Hazenkamp, H.U. Gudel, M. Atanasov, U. Kesper, D. Reinen, Phys Rev. B 1996;53:2367

Table 1
Crystallographic parameters of Cr-doped $Y_2Ti_2O_7$ pyrochlores

	PT00	PT02	PT07	PT25	PT50	PT75	PT100
Rietveld refinement							
R_{wp}	0.04	0.12	0.13	0.12	0.11	0.12	0.11
R_{Bragg}	0.04	0.04	0.04	0.03	0.02	0.02	0.02
No. of data	6000	9035	9035	9035	9035	9035	8985
No. of reflections	122	122	122	122	122	122	122
Phase composition							
pyrochlore (% wt.)	100.0(1)	100.0(1)	99.6(2)	90.6(5)	77.4(5)	64.5(5)	51.2(5)
$YCrO_3$ perovskite (% wt.)	0.0	0.0	0.4(2)	9.5(5)	22.6(5)	35.5(5)	48.8(5)
Pyrochlore unit cell parameters							
Unit cell dimension a (Å)	10.0987 7(5)	10.0979 0(4)	10.0963 3(4)	10.0990 4(4)	10.0963 0(4)	10.0957 7(4)	10.0960 0(5)
Unit cell volume (Å^3)	1029.93	1029.66	1029.18	1030.01	1029.20	1029.01	1029.10
x(O)	.3277(3)	.32005(9)	.32006(7)	.32010(6)	.32012(6)	.32002(7)	.32011(9)
A-O distance (Å)	2.493(3)	2.4832(6	2.4827(5	2.4825(4	2.4823(4	2.4829(5	2.4823(6
A-O’ distance (Å)	2.186(1)	2.1863(3	2.1859(2	2.1865(2	2.1859(2	2.1858(2	2.1859(3
B-O distance (Å)	1.950(1)	1.9554(4	1.9552(2	1.9562(2	1.9554(2	1.9549(3	1.9553(4
A occupancy (Y)	1.00	1.00	1.00	1.00	1.00	1.00	1.00
B occupancy (Ti)	1.00	1.00	0.993(3)	0.958(2)	0.947(2)	0.942(3)	0.952(4)
B occupancy (Cr)	0.00	0.00	0.007(3)	0.042(2)	0.053(2)	0.058(3)	0.048(4)
O occupancy	1.00	1.00	1.00	1.00	1.00	1.00	1.00
O’ occupancy	1.00	1.00	1.00	1.00	1.00	1.00	1.00
Perovskite unit cell parameters							
a (Å)	-	-	-	5.5249(2	5.5234(1	5.5231(1	5.5225(1
b (Å)	-	-	-	7.5366(2	7.5379(1	7.5383(1	7.5386(1
c (Å)	-	-	-	5.2445(1	5.2457(1	5.2461(1	5.2465(1
Volume (Å^3)	-	-	-	218.38	218.40	218.42	218.42

Notes: All results from combined X-ray/neutron refinements except PT00 which is from X-ray data only. Figures in parentheses are standard deviations in the last decimal figure.
Meanings of the column headings: R_{Bragg} as well as the number of reflections is referred only to pyrochlore. R_{Bragg}. R_{wp} and phase composition are the mathematical average of the X-ray and neutron value while the number of reflections is the X-ray one.

Table 2
Crystallographic parameters of Cr-doped $Y_2Sn_2O_7$ pyrochlores

	PS00	PS02	PS07	PS25	PS50	PS75	PS100
Rietveld refinement							
R_{wp}	0.17	0.12	0.12	0.12	0.11	0.11	0.10
R_{Bragg}	0.06	0.04	0.03	0.03	0.03	0.03	0.03
No. of data	6000	8884	8845	8845	8845	8845	8843
No. of reflections	130	130	130	130	130	130	130
Phase composition							
pyrochlore (% wt.)	100.0	100.0	100.0	94.9(1)	85.0(1)	73.0(1)	61.3(1)
$YCrO_3$ perovskite (%	0.0	0.0	0.0	5.1(1)	15.0(1)	27.0(1)	38.7(1)
Pyrochlore							
Unit cell dimension *a*	10.3753	10.3730	10.3684	10.3634	10.3615	10.3611	10.3609
Unit cell volume (Å^3)	1116.89	1116.13	1114.65	1113.04	1112.42	1112.30	1112.26
x(O)	0.3350(5	0.33662(	0.33665(	0.33645(	0.33646(	0.33650(	0.33645(
A-O distance (Å)	2.509(3)	2.4970(5	2.4956(3	2.4958(4	2.4953(5	2.4949(6	2.4952(7
A-O’ distance (Å)	2.246(1)	2.2458(2	2.2448(1	2.2437(1	2.2433(2	2.2432(2	2.2432(3
B-O distance (Å)	2.035(2)	2.0420(3	2.0412(2	2.0393(3	2.0390(3	2.0391(4	2.0389(5
A occupancy (Y)	1.00	1.00	1.00	1.00	1.00	1.00	1.00
B occupancy (Sn)	1.00	0.978(5)	0.970(5)	0.968(5)	0.939(5)	0.938(5)	0.921(5)
B occupancy (Cr)	0.00	0.022(5)	0.030(5)	0.032(5)	0.061(5)	0.062(5)	0.079(5)
O occupancy	1.00	0.987(2)	0.987(5)	0.985(6)	0.984(7)	0.985(8)	0.982(9)
O’ occupancy	1.00	1.00	1.00	1.00	1.00	1.00	1.00
Perovskite unit cell parameters							
a (Å)	-	-	-	-	5.5210(2	5.5222(1	5.5221(1
b (Å)	-	-	-	-	7.5382(2	7.5377(1	7.5378(1
c (Å)	-	-	-	-	5.2468(2	5.2462(1	5.2462(1
Volume (Å^3)	-	-	-	-	218.36	218.37	218.37

Notes: All results from combined X-ray/neutron refinements except PS00 which is from X-ray data only. Figures in parentheses are standard deviations in the last decimal figure.
Meanings of the column headings: R_{Bragg} as well as the number of reflections is referred only to pyrochlore. R_{Bragg}. R_{wp} and phase composition are the mathematical average of the X-ray and neutron value while the number of reflections is the X-ray one.

Table 3
Diffuse reflectance data of Cr-doped titanate and stannate pyrochlores

Sample	PYROCHLORE										
	Band υ_1			Band υ_2			Band υ_3			Ratios	
	ϖ (cm^{-1})	δ (cm^{-1})	area (a.u.)	ϖ (cm^{-1})	δ (cm^{-1})	area (a.u.)	ϖ (cm^{-1})	δ (cm^{-1})	area (a.u.)	υ_1/υ_2	υ_3/υ_1
PT02	18280	5330	2760	25530	9320	5580	10450	1640	50	0.49	0.02
PT07	17230	4760	3110	23520	9510	9060	10360	1110	30	0.34	0.01
PT25	17410	3820	2200	25400	5980	4010	10690	2190	100	0.55	0.05
PT50	16940	3580	1550	25800	7760	5780	10750	2330	130	0.27	0.08
PT75	17920	4210	2240	26500	5280	3480	10740	1970	80	0.64	0.04
PT100	17800	4330	2200	26680	5860	4170	10740	2050	90	0.53	0.04
PS02	18330	5400	2920	25400	8590	5110	10470	1780	50	0.57	0.02
PS07	18300	5260	3210	25920	10220	7770	10590	2040	150	0.41	0.05
PS25	18420	4200	3060	25640	5150	3920	10710	2160	250	0.78	0.08
PS50	18360	4040	2690	25800	5440	4070	10710	2190	270	0.66	0.10
PS75	18290	4050	2380	25790	6540	4940	10720	2100	240	0.48	0.10
PS100	18440	4460	2660	25930	5720	3760	10720	2020	200	0.71	0.07

Sample	PEROVSKITE										
	Band υ_1			Band υ_2			^2E		$^2T_1$		Ratio
	ϖ (cm^{-1})	δ (cm^{-1})	area (a.u.)	ϖ (cm^{-1})	δ (cm^{-1})	area (a.u.)	ϖ (cm^{-1})	δ (cm^{-1})	ϖ (cm^{-1})	δ (cm^{-1})	υ_1/υ_2
PT25	15350	2650	880	20780	4860	2910	13920	870	14470	650	0.30
PT50	15300	2720	690	20110	5820	3660	13840	830	14670	930	0.19
PT75	15720	3100	1210	21780	5270	3710	13750	720	14460	740	0.32
PT100	15730	3240	1130	21670	5320	3660	13730	710	14530	820	0.31
PS25	15900	2560	560	21560	4270	2030	13950	750	14520	620	0.28
PS50	15950	2750	730	21470	4620	2480	13790	680	14500	720	0.29
PS75	16000	2910	780	21180	4560	2130	13750	650	14460	680	0.37
PS100	15990	3070	740	21740	4390	2090	13730	640	14470	680	0.35
$YCrO_3$	16400	2570	1340	22380	5310	3970	13610	490	14300	990	0.34

Table 4
Spectroscopic parameters of Cr-doped titanate and stannate pyrochlores

Sample	Pyrochlore			Perovskite				
	Δ_o (cm^{-1})	B (cm^{-1})	β (1)	Δ_o (cm^{-1})	B_{35} (cm^{-1})	β_{35} (1)	B_{55} (cm^{-1})	β_{55} (1)
PT02	19730	650	0.63	-	-	-	-	-
PT07	18510	660	0.64	-	-	-	-	-
PT25	18820	700	0.67	15610	525	0.58	365	0.40
PT50	18270	770	0.74	15330	450	0.49	440	0.48
PT75	19350	750	0.72	16170	600	0.66	420	0.45
PT100	19160	780	0.75	16130	585	0.64	440	0.48
PS02	19770	640	0.62	-	-	-	-	-
PS07	19710	685	0.66	-	-	-	-	-
PS25	19840	655	0.63	16180	545	0.60	375	0.41
PS50	19830	665	0.64	16170	530	0.58	415	0.45
PS75	19740	670	0.64	16080	490	0.54	415	0.45
PS100	19830	680	0.65	16290	560	0.61	425	0.46
$YCrO_3$	-	-	-	16740	580	0.64	420	0.46

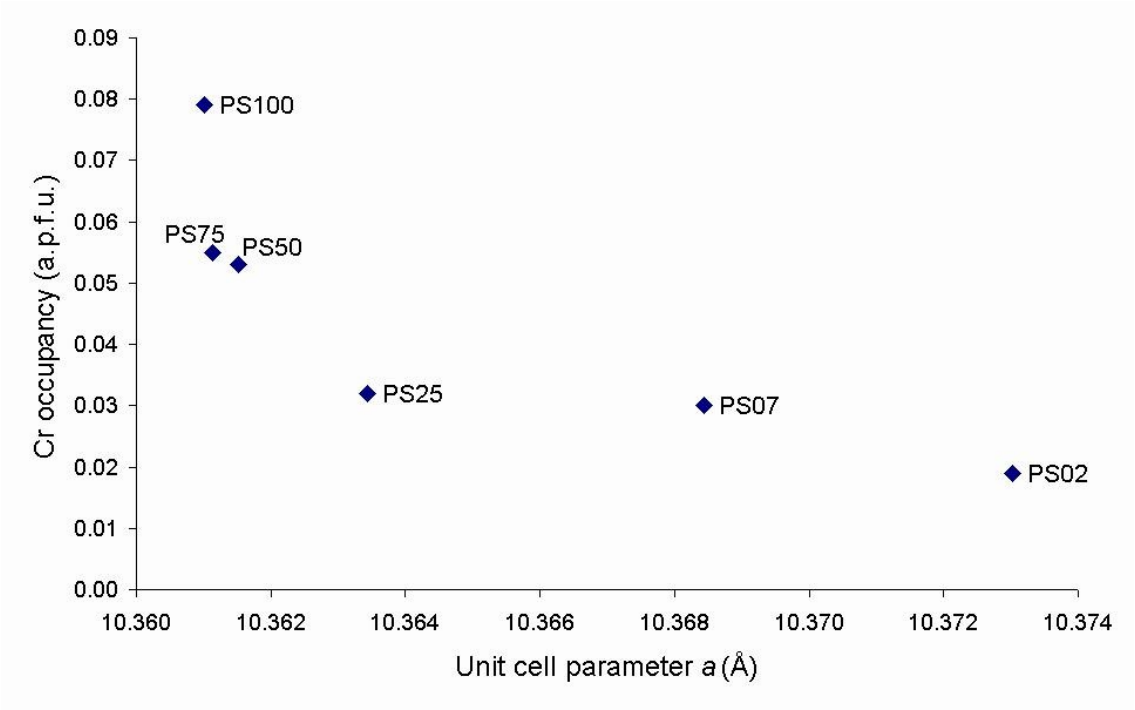

Fig. 1. Unit cell parameter *a* as a function of the refined Cr content in the PS pyrochlores. The error was in all cases <0.0001 Å.

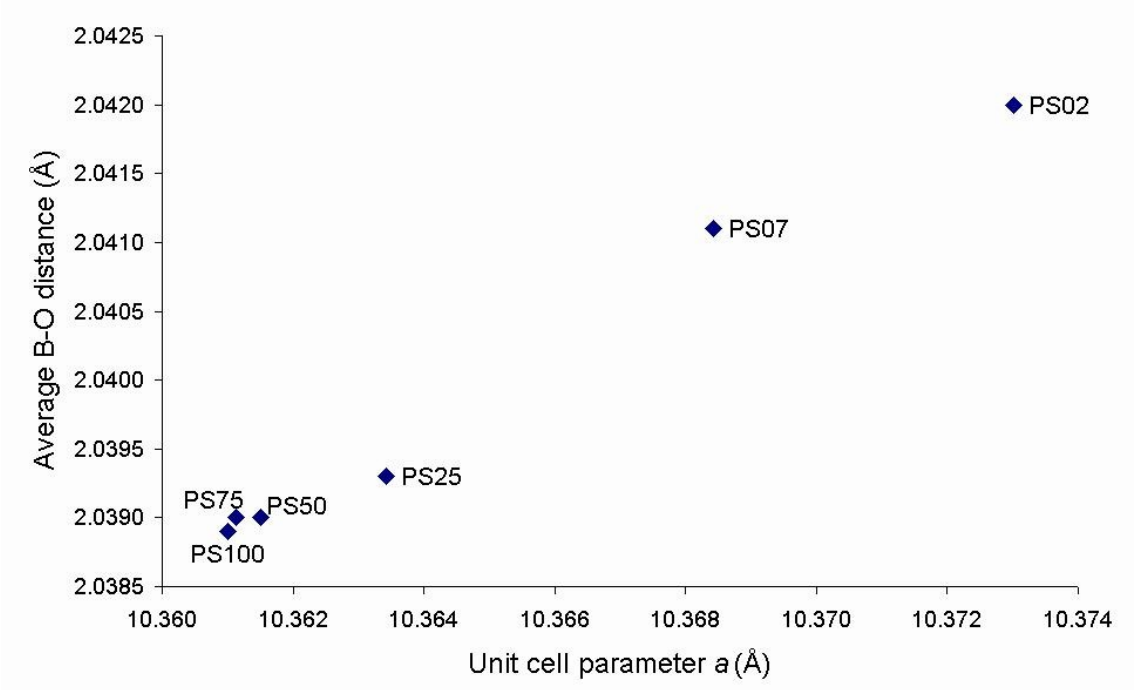

Fig. 2. Unit cell parameter *a* as a function of the average refined <B-O> distance in the PS pyrochlores.

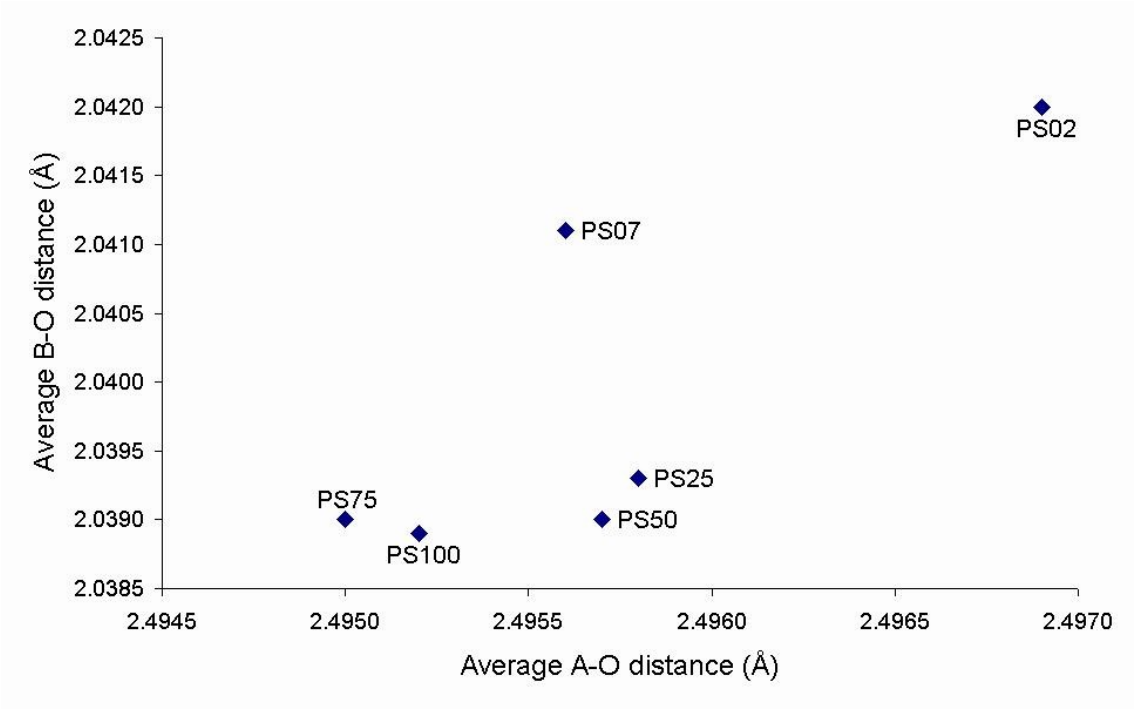

Fig. 3. Average B-O distance versus average A-O distance in the PS pyrochlores. The error was in all cases <0.001 Å.

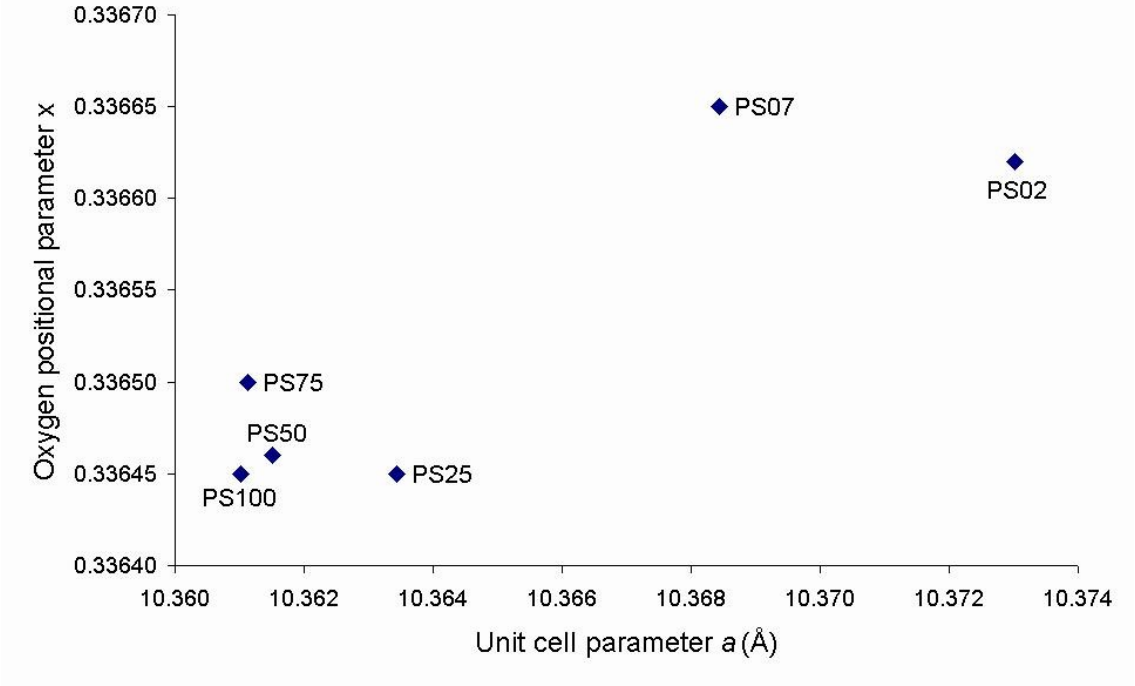

Fig. 4. Variation of the oxygen positional parameter, x, with the unit cell parameter *a* in the PS pyrochlores.

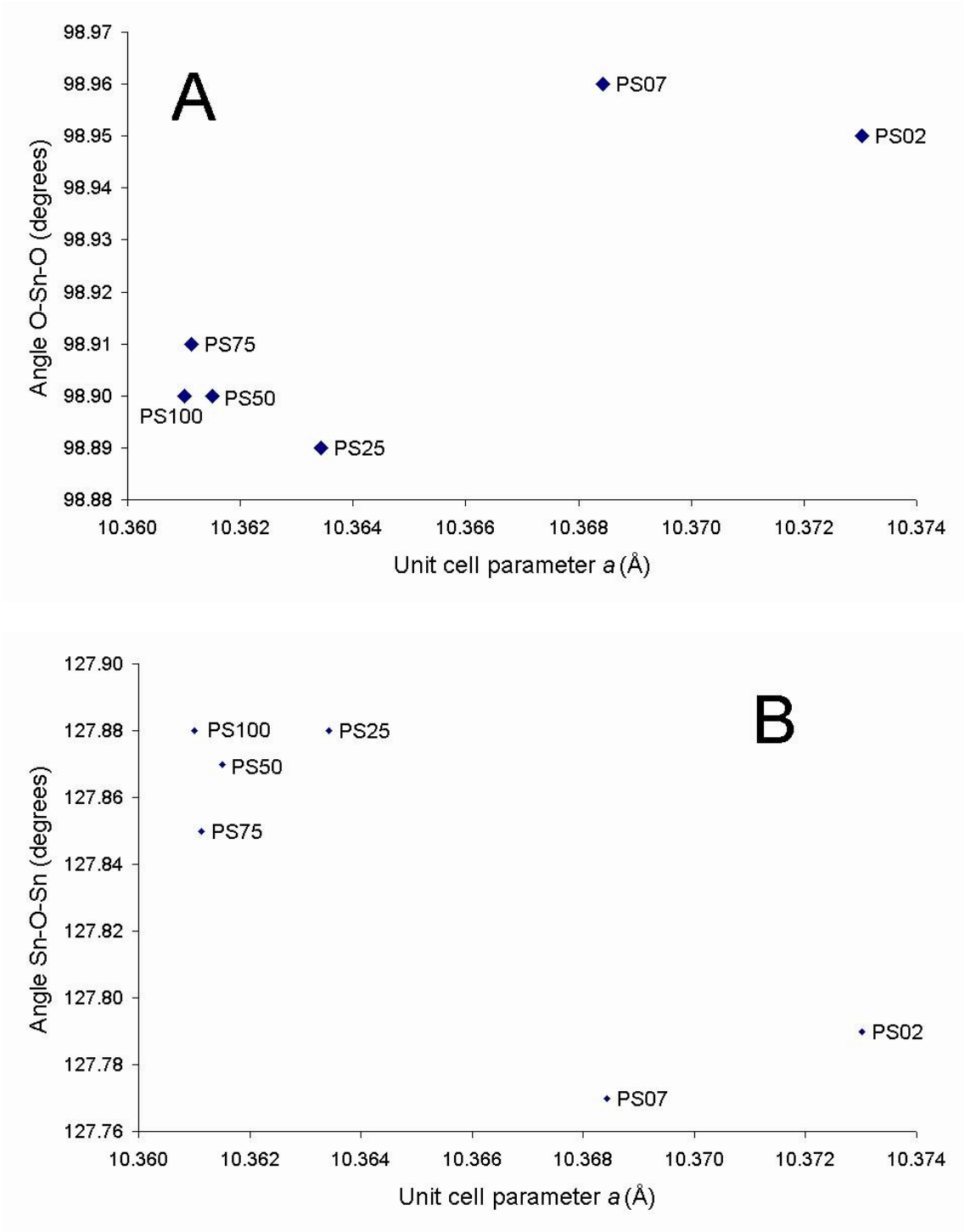

Fig. 5. Variation of the O-Sn-O (A) and Sn-O-Sn (B) bond angles with the unit cell parameter *a* in the PS pyrochlores.

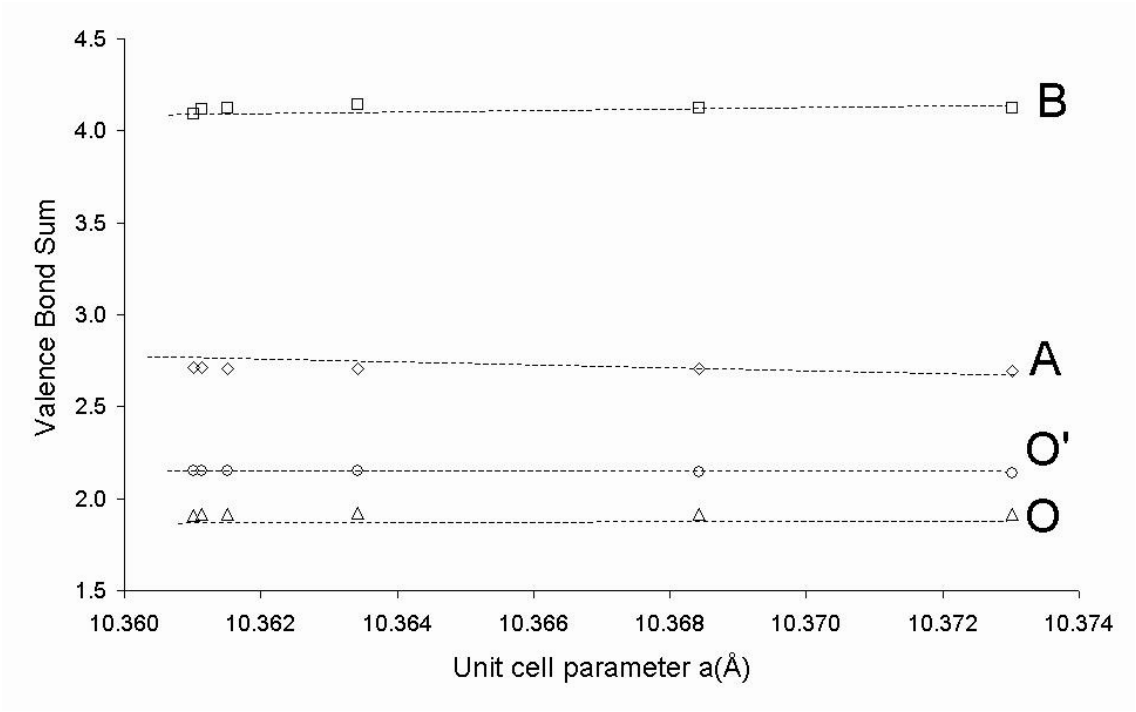

Fig. 6. Variation of bond valence sums (BVS) at the A, B, O and O' sites as a function of the unit cell parameter *a* [increasing with decreasing Cr content] in the PS pyrochlores.

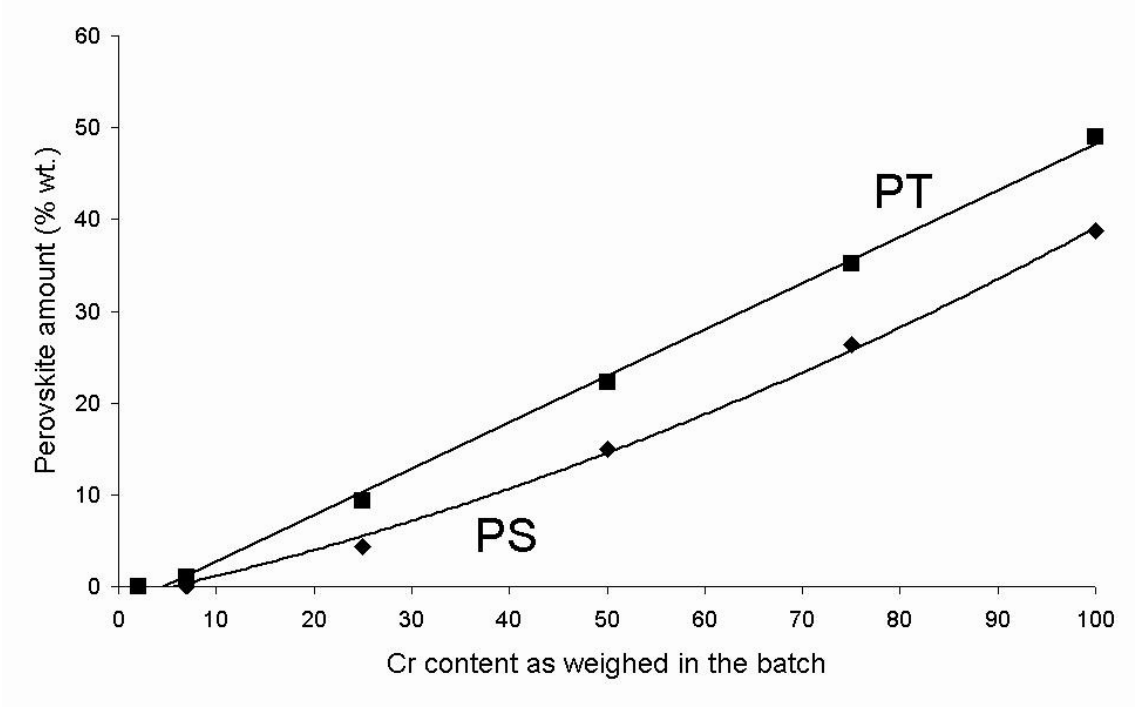

Fig. 7. Pervovskite amount (% wt.) as a function of the Cr amount added in the batch.

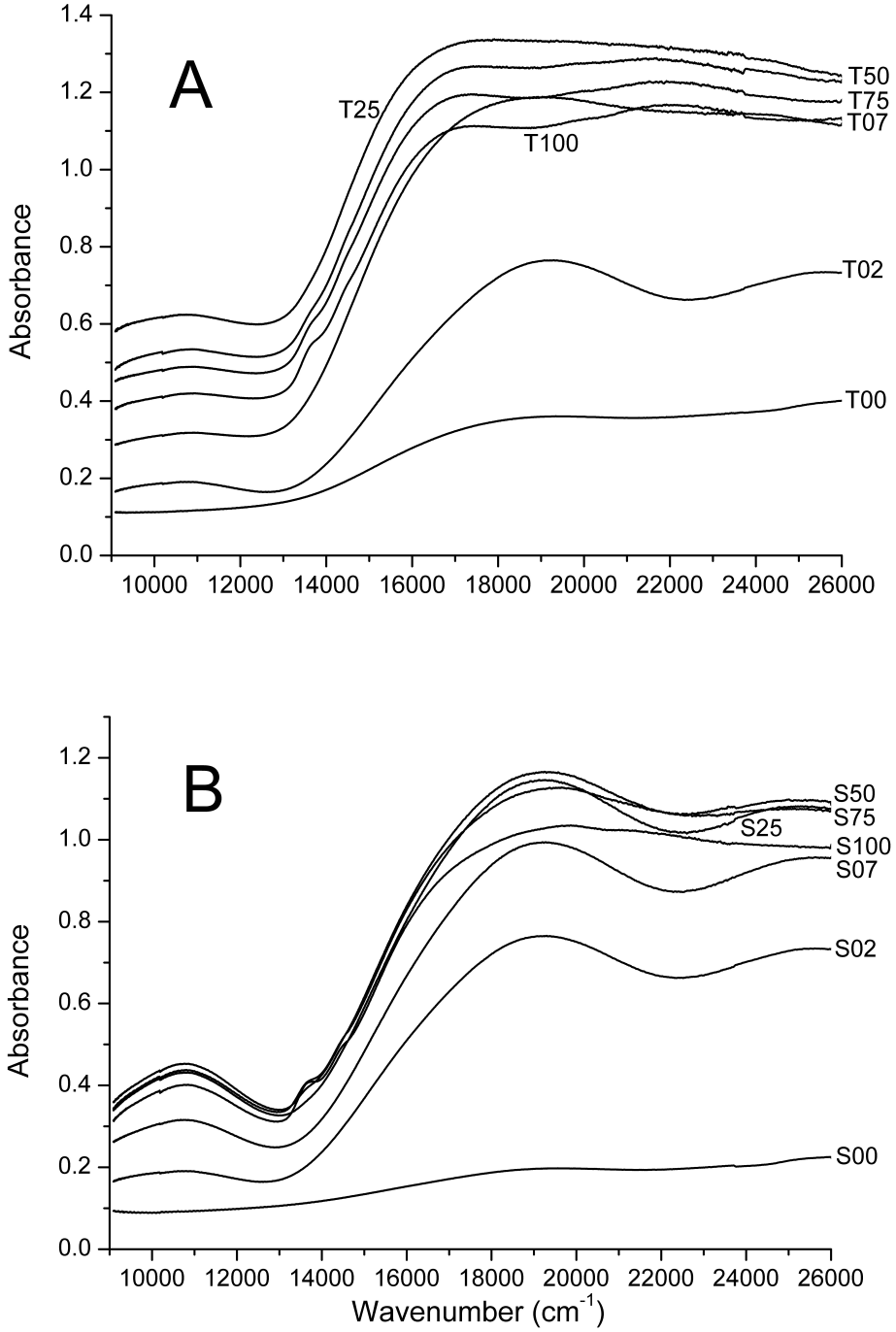

Fig. 8. Optical spectra of the PT (A) and PS (B) pigments.

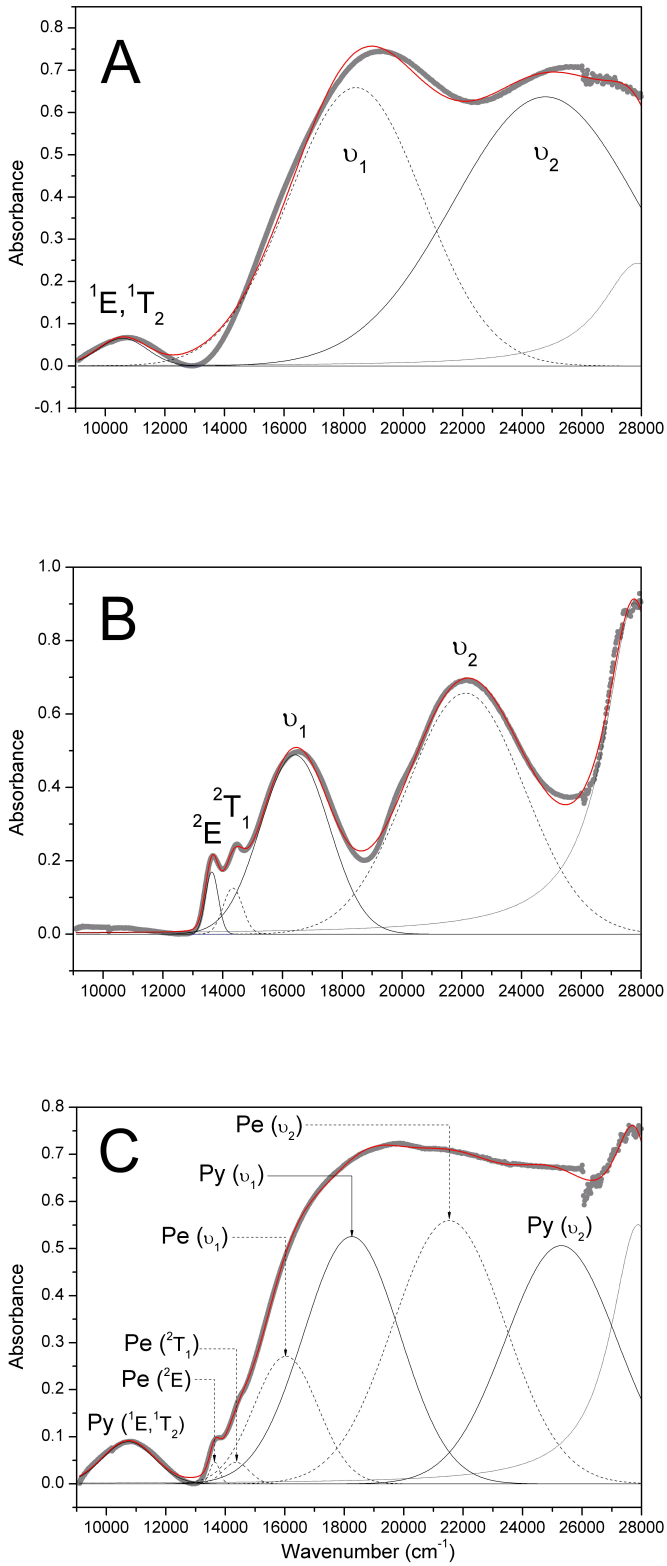

Fig. 9. Deconvoluted optical spectra of the PS0 (A), $YCrO_3$ (B), and PS100 (C) samples. See text for the attribution of optical bands.

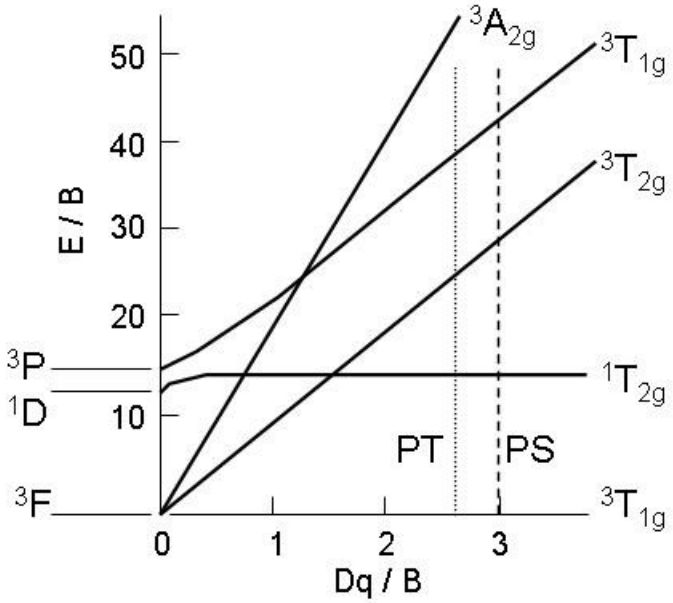

Fig. 10. Energy level plot of Cr^{4+} (d^2 ion) with average crystal field strength of the PT and PS series.